BIOLOGY OF REPRODUCTION (2016) **95**(2):44, 1–16
Published online before print 22 June 2016.
DOI 10.1095/biolreprod.116.139477

SMAD Signaling Is Required for Structural Integrity of the Female Reproductive Tract and Uterine Function During Early Pregnancy in Mice[1]

Amanda Rodriguez,[3,4,5] Swamy K. Tripurani,[3,4] Jason C. Burton,[6] Caterina Clementi,[4,7] Irina Larina,[8] and Stephanie A. Pangas[2,4,9,10]

[4]*Department of Pathology and Immunology, Baylor College of Medicine, Houston, Texas*
[5]*Graduate Program in Molecular and Cell Biology, Baylor College of Medicine, Houston, Texas*
[6]*Graduate Program in Integrative Molecular and Biomedical Sciences, Baylor College of Medicine, Houston, Texas*
[7]*Graduate Program in Developmental Biology, Baylor College of Medicine, Houston, Texas*
[8]*Department of Molecular Physiology and Biophysics, Baylor College of Medicine, Houston, Texas*
[9]*Department of Molecular and Cellular Biology, Baylor College of Medicine, Houston, Texas*
[10]*Center for Reproductive Medicine, Baylor College of Medicine, Houston, Texas*

ABSTRACT

Pregnancy is a complex physiological process tightly controlled by the interplay among hormones, morphogens, transcription factors, and signaling pathways. Although recent studies using genetically engineered mouse models have revealed that ligands and receptors of transforming growth factor beta (TGFbeta) and bone morphogenetic protein (BMP) signaling pathways are essential for multiple reproductive events during pregnancy, the functional role of SMAD transcription factors, which serve as the canonical signaling platform for the TGFbeta/BMP pathways, in the oviduct and uterus is undefined. Here, we used a mouse model containing triple conditional deletion of the BMP receptor signaling *Smads* (*Smad1* and *Smad5*) and *Smad4*, the central mediator of both TGFbeta and BMP signaling, to investigate the role of the SMADs in reproductive tract structure and function in cells from the *Amhr2* lineage. Unlike the respective single- or double-knockouts, female *Smad1*$^{flox/flox}$ *Smad5*$^{flox/flox}$ *Smad4*$^{flox/flox}$ *Amhr2*$^{cre/+}$conditional knockout (*i.e., Smad1/5/4-Amhr2-cre* KO) mice are sterile. We discovered that *Smad1/5/4-Amhr2-cre* KO females have malformed oviducts that subsequently develop oviductal diverticuli. These oviducts showed dysregulation of multiple genes essential for oviduct and smooth muscle development. In addition, uteri from *Smad1/5/4-Amhr2-cre* KO females exhibit multiple defects in stroma, epithelium, and smooth muscle layers and fail to assemble a closed uterine lumen upon embryo implantation, with defective uterine decidualization that led to pregnancy loss at early to mid-gestation. Taken together, our study uncovers a new role for the SMAD transcription factors in maintaining the structural and functional integrity of oviduct and uterus, required for establishment and maintenance of pregnancy.

fertility, mouse models, ovary, oviduct, pregnancy, uterus

INTRODUCTION

Early pregnancy loss is a common occurrence in women and often occurs due to defects during pre-, peri-, and post-implantation periods [1, 2]. In natural conception, the chance of a successful pregnancy occurring in a given menstrual cycle is limited to approximately 30%, and only 50% to 60% of all conceptions advance beyond 20 weeks of gestation [2]. Of those pregnancies that are lost, 75% fail to implant and are not clinically recognized [2]. Multiple factors contribute to implantation failure, including poor embryo quality (e.g., chromosomal abnormalities) or endocrine disturbances resulting in abnormal embryo spacing, decidualization, placentation, and intrauterine embryonic growth [3, 4]. However, in most cases, the cause of implantation failure is unexplained. Defects in fallopian tube structure as well as function can also result in infertility [5]. Recent progress using genetically engineered mouse models indicates that ovarian hormones together with locally produced signaling molecules, including cytokines, growth factors, homeobox transcription factors, lipid mediators, and morphogen genes function through autocrine, paracrine, and juxtacrine interactions to specify the complex processes of embryo implantation and establishment of the uterus-embryo axis during postimplantation period [6, 7]. Because embryo implantation is a dynamic developmental process that integrates multiple signaling molecules into a precisely orchestrated program, it is important to understand the hierarchical landscape of molecular signaling pathways that govern the embryo-uterus interaction in order to generate new strategies to correct and/or identify the causes of implantation failure and improve pregnancy outcome, including pregnancies conceived through assisted reproductive techniques.

Proteins of the transforming growth factor β (TGFβ) superfamily are evolutionarily conserved and essential mediators of cellular growth and differentiation. Members of this family are secreted and bind to type 2 and type 1 cell surface receptors that activate the SMAD transcription factors as the canonical signaling pathway [8]. Based on sequence similarities, the TGFβ superfamily is grossly divided into two main ligand subfamilies: the TGFβ-activin-nodal subfamily and the BMP subfamily [8]. TGFβ, activin, and nodal signal through SMAD2 and SMAD3 (termed AR-SMADs), whereas the bone morphogenetic proteins (BMPs) use SMAD1 and SMAD5

[1]Supported by U.S. National Institutes of Health grants R01 CA138628, R01 HD076980, T32 HD007165, R01 HL120140, T32 GM008231, and P30 CA125123 and a Burroughs Wellcome Career Award in the Biomedical Sciences.
[2]Correspondence: Stephanie A. Pangas, Baylor College of Medicine Pathology, One Baylor Plaza, Mailstop BCM 315, Houston, TX 77030. E-mail: spangas@bcm.edu
[3]These authors contributed equally to this work.

Received: 12 February 2016.
First decision: 29 March 2016.
Accepted: 10 June 2016.

eISSN: 1529-7268 http://www.biolreprod.org
ISSN: 0006-3363

TABLE 1. Summary of major female reproductive phenotypes in SMAD conditional KO mouse models.[a]

Mouse model	Pups/litter[b]	Litters/month[b]	Oviduct diverticuli phenotype	Reference
Background Colony	8.3 ± 0.3	1.0 ± 0.0	No	[18]
Smad1-Amhr2-cre	10.2 ± 0.4	1.1 ± 0.0	No	[18]
Smad4-Amhr2-cre	1.3 ± 0.4*	0.5 ± 0.1*	No	[27]
Smad5-Amhr2-cre	7.3 ± 0.3	1.0 ± 0.1	No	[18]
Smad1/5-Amhr2-cre	3.6 ± 0.8*	0.6 ± 0.2*	No	[18]
Smad1/5/4-Amhr2-cre	0.0 ± 0.0*	0.0 ± 0.0*	Yes	[24]

[a] Fertility analyses of *Smad* conditional KOs generated with *Amhr2-cre* as previously published. [b] Pups per litter and litters per month are shown as averages ± SEM.
* Significantly different from controls, $P < 0.05$.

(termed BR-SMADs). Both of these pathways share SMAD4 (the ''common'' SMAD) to form trimeric protein complexes to initiate signal transduction [9]. Several studies have clearly demonstrated that members of TGFβ superfamily regulate diverse developmental and homeostatic processes and are mutated in numerous human diseases including cancer and infertility [9, 10]. Studies using genetically engineered mouse models demonstrate that ligands and receptors of TGFβ and BMP signaling pathway display spatiotemporal expression patterns in reproductive tissues and are critically involved in multiple reproductive events including germ cell specification, folliculogenesis, embryo implantation, uterine decidualization, and placental development [11, 12]. For instance, progesterone receptor (*Pgr*) promoter-driven *Cre* recombinase-mediated conditional deletion of *Bmp2* [13], the BMP receptor type I (*Bmpr2*) [14] or the BMP type 1 receptor, activin-like kinase 2 (*Alk2*) [15] in the uterine epithelium results in infertility due to abnormalities in uterine functions, including implantation, decidualization, vascular development, and trophoblast invasion during pregnancy. However, ablation of *Alk2* in the uterine stromal and myometrial compartment, using anti-Müllerian hormone receptor type 2 (*Amhr2*) promoter-driven *Cre* recombinase, does not affect fertility. In contrast, conditional deletion of the TGFβ type I receptor (*Tgfbr1)* by using *Amhr2-cre* results in sterility primarily through developmental defects in smooth muscle layers of the oviduct and uterus [16]. Together, these results indicate the compartment-specific (i.e., epithelial/stromal/myometrial) functional role of these genes and highlight the importance of compartment-specific deletion for better understanding the role of TGFβ and BMP signaling pathway during reproductive events.

Mouse models for studying the SMAD transcription factors in pregnancy are limited due to early embryonic lethality of the SMAD homozygous null mutations and are complicated by genetic redundancy between the AR-SMADs or BR-SMADs [17, 18]. *Smad4*-null embryos arrest during gastrulation at approximately Embryonic Day (E) 7.5 [19], whereas *Smad1* null or *Smad5* null die at midgestation [17, 20]. Our laboratory has been using tissue-specific conditional gene inactivation by using *Cre-loxP* technology to expand the understanding of reproductive functions of SMAD transcription factors (Table 1). Disruption of *Smad4* using *loxP*-flanked alleles and *Amhr2-cre* leads to premature luteinization of ovarian follicles; in contrast, oocyte-specific deletion of *Smad4* with the zona pellucida 3 (*Zp3*)-*cre* gene or growth differentiation factor 9 (*Gdf9*)-*icre* driver lines causes minimal fertility defects in mice but disrupts primordial follicle numbers [21]. *Amhr2-cre*-mediated deletion of the AR-SMADs (SMAD2 and SMAD3) revealed redundant roles of *Smad2* and *Smad3* in multiple ovarian processes, including follicular development, ovulation, and cumulus cell expansion [22], but no reported uterine defects. Furthermore, double conditional knockout (KO) of *Smad1* and *Smad5* using *Amhr2-cre* reduces litter sizes and causes metastatic granulosa cell tumors [18, 23] (Table 1).

Recently, we generated a triple conditional SMAD KO mouse model by genetically deleting *Smad4* from *Smad1 Smad5* double-KO mice in the female reproductive tract, using *Amhr2-cre* [24]. We had generated this mouse model to analyze the role of *Smad4* in granulosa cell tumorigenesis. During these studies, we found that surprisingly, *Smad1*/*5*/*4-Amhr2-cre* KO mice were sterile, unlike the single or double *Smad1-Amhr2-cre* KO, *Smad5-Amhr2-cre* KO, *Smad1*/*5-Amhr2-cre* KO, or *Smad4-Amhr2-cre* KO mice [24] (Table 1). Our initial findings indicated that the sterility of *Smad1*/*5*/*4-Amhr2-cre* KO females was not fully caused by defects in ovarian function [24], so in this study, we further analyzed the reproductive tract where *Amhr2-cre* is known to be expressed, that is, in the developing Müllerian ducts as well as the smooth muscle compartments of the oviduct, myometrium, and stroma of uteri in adult mice [25, 26]. We found that *Smad1*/*5*/*4-Amhr2-cre* KO mice have a striking oviductal and uterine phenotype that has not been previously observed in any SMAD mutant mouse models that used *Amhr2-cre*, thereby uncovering a novel role of SMAD signaling in female reproductive tract development and uterine function. Furthermore, to our knowledge, this is the first study to use the imaging technique of optical coherence tomography for a structural analysis of the reproductive tract in a mouse mutant.

MATERIALS AND METHODS

Animals

Experimental animals were used in accordance with the National Institutes of Health Guide for the Care and Use of Laboratory Animals and with institutionally approved animal protocols at Baylor College of Medicine. Generation and initial characterization of $Smad1^{flox/flox}$ $Smad5^{flox/flox}$ $Smad4^{flox/flox}$ $Amhr2^{cre/+}$ (referred to throughout as *Smad1*/*5*/*4-Amhr2-cre* KO or *Smad1*/*5*/*4 tKO*) was described previously [24]. Experimental animals were maintained on a *C57BL*/*6J*/*129S7*/*SvEvBrd* mixed hybrid background. Mice were genotyped using tail genomic DNA and PCR as reported previously [18, 27]. Littermates that were wild type at the *Amhr2* locus served as controls (*e.g.*, $Smad1^{flox/flox}$ $Smad5^{flox/flox}$ $Smad4^{flox/flox}$ or their respective single or double lines as appropriate). To control for potential background differences between colonies, we rederived the *Smad1*/*5-Amhr2-cre* (double-KO) and *Smad4-Amhr2-cre* (single-KO) females directly from the *Smad1*/*5*/*4-Amhr2-cre* KO colony.

Fertility Analysis

Fertility of mice was monitored as previously described [18, 27]. Fertility was previously reported in the initial description of each knockout line as shown in Table 1. At 6 wk of age, female control and KO mice were housed individually with wild-type males of proven fertility. Mice were kept in mating pairs for 6 mo with cage enrichment, and the number of pups per litter and litters per month were recorded.

Superovulation

Three- to 4-wk-old control and *Smad1*/*5*/*4-Amhr2-cre* KO females were given i.p. injections of 5 IU of pregnant mare serum gonadotropin (EMD Millipore) for 44 to 46 h, followed by injection of 5 IU of human chorionic gonadotropin (Novarel; Ferring Pharmaceuticals) for 18 h. To collect cumulus-oocyte complexes (COC), the COC were released from the ampulla of the oviduct into minimum essential medium containing bovine hyaluranidase to separate cumulus cells from oocytes for counting. For optical coherence tomography (OCT) imaging, reproductive tracts were dissected intact and imaged (see *Optical Coherence Tomography Imaging*).

Tissue Collection and Histological Analysis

Mice were anesthetized by isoflurane inhalation (Butler Schein) and euthanized by cervical dislocation prior to tissue collection. For histological studies, oviduct and uterus samples from mice were dissected and fixed in 10% neutral buffered formalin overnight at room temperature. After fixation, formalin-fixed samples were transferred to 70% ethanol for long-term storage at room temperature or processed for embedding. Tissue processing and paraffin embedding were performed by the Human Tissue Acquisition and Pathology Core Services facility at Baylor College of Medicine. Histological sections were cut at 5 μm and stained with hematoxylin and eosin or periodic acid–Schiff (PAS) reaction, using standard procedures. For total RNA isolation, tissue sections were collected and stored in RNAlater solution (Life Technologies) overnight at 4°C to allow thorough penetration of the tissue and then frozen to −80°C for long-term storage or until RNA extraction.

Artificial Induction of Decidualization

The artificial induction of decidualization of the uterus was performed as previously described [28]. Briefly, 8-wk-old control and *Smad1/5/4-Amhr2-cre* KO mice were ovariectomized via a dorsal incision under anesthesia, and mice were allowed to recover for 2 wk to achieve complete withdrawal of endogenous ovarian hormones. After 2 wk, mice were ''primed'' with subcutaneous injections of 100 ng of 17β-estradiol (E2) once a day for 3 days. After 2 days, mice were treated daily for 3 days with subcutaneous injections of 1 mg of progesterone (P4) and 6.7 ng of E2 per mouse. One uterine horn was then stimulated to decidualize by traumatizing (''scratching'') the entire length of the uterine endometrium with a large needle 6 h after the last hormone injection. The contralateral horn was left untreated and served as a control. Each day after the decidual stimulus, mice were given subcutaneous injections of 1 mg of P4 and 6.7 ng of E2 per mouse. On the second and fifth days after the decidual stimulus, mice were euthanized 6 h after the last hormone injection. Uterine horns were collected, and the wet weights of the stimulated and control horns were recorded, and tissue was processed for histological and molecular analysis.

Alkaline Phosphatase Staining

Uteri that had undergone artificial decidualization were fixed in 4% paraformaldehyde overnight and immersed in 10% to 30% sucrose solution prior to embedding in optimal cutting temperature compound. Ten-micrometer tissue sections were post-fixed in 0.2% glutaraldehyde and washed in phosphate-buffered saline (PBS). The 5-bromo-4-chloro-3-indoyl phosphate/nitroblue tetrazolium alkaline phosphotase (BCIP/NBT AP) substrate (Vector) was prepared according to the manufacturer's instructions. Tissues were incubated with the substrate solution for 25 min and rinsed in tap water, nuclei were counterstained with nuclear fast red, and slides were mounted (VectaMount AQ mounting medium; Vector). A dark blue colorimetric reaction indicated stromal cell differentiation.

Optical Coherence Tomography Imaging

For volumetric structural analysis of the reproductive tract, we used a custom-built spectral-domain OCT system that has been described previously [29]. Briefly: the system uses a low-coherence Ti:sapphire laser source (Micra-5; Coherence, Inc.) with a central wavelength of ~808 nm, a bandwidth of ~110 nm, and a power output of ~400 nm. The setup uses a Michelson interferometer to generate interference fringes from the backscattered light collected from the sample and reference arms. The fringes are resolved using a custom-built spectrometer and are converted into in-depth intensity profiles using fast-Fourier transform. The system provides a lateral resolution of ~4 μm and an axial resolution of ~5 μm. The A-line (in-depth intensity profile) scan rate was set at 50 kHz. Due to light attenuation in tissue, the imaging depth in reproductive organs is limited to ~1 to 1.5 mm. For the imaging, reproductive tracts were dissected and placed in a dish with PBS. Freshly excised tissues were imaged with OCT in PBS without any staining. After tissues were imaged, they were collected for further analysis. Data rendering and three-dimensional (3D) visualizations were performed using Imaris software (Bitplane, Switzerland).

Analysis of Implantation

Success of implantation was determined by counting implantation sites at indicated times during early pregnancy (E4.5–E9.5). Eight-wk-old female control and experimental mice were allowed to naturally mate with wild-type males and were examined daily in the morning for the presence of seminal plug; the morning of plug detection was considered E0.5. Implantation of embryos was evaluated at E4.5, E5.5, E6.5, E7.5, and E9.5. For E4.5, implantation sites were visualized by intravenous injection of Chicago Blue dye and euthanized 2 minutes after dye injection [15].

RNA Extraction, Reverse Transcription and Quantitative Real-Time PCR

Total RNA from the oviduct and uterus were extracted using RNeasy micro- or mini-kit (Qiagen) according to the manufacturer's instructions. RNA concentrations were measured using a spectrophotometer (model ND 1000; NanoDrop Technologies). Reverse transcription was carried out using 200 ng of total RNA, using High-Capacity RNA-to-cDNA Master Mix (Life Technologies) according to the manufacturer's instructions. Real-time quantitative PCR (qPCR) was performed using custom-designed primers and Fast SYBR Green Master Mix (Life Technologies). Primer information used in this study is listed in Supplemental Table S1 (Supplemental Data are available online at www.biolreprod.org). All qPCR assays were performed in triplicate for each sample, using a minimum of three mice per group. Melt curve analysis was performed to verify a single amplification peak for determining the specificity of amplification. Relative mRNA levels of transcript were calculated by the cycle threshold (ΔΔCT) method as described previously [30] and were normalized to the endogenous reference (*Gapdh* or *Rpl19*), as indicated in the text. The expression data are presented as relative values ± standard errors of the mean (SEM), using the control mean as the calibrator (set to equal 1) as described previously [31].

Immunofluorescence and TUNEL Assay

Paraffin-embedded sections were deparaffinized in xylene and rehydrated in a graded alcohol series. Antigen retrieval was performed by boiling the sections in a 10 mM sodium citrate antigen unmasking buffer with 0.05% Tween 20 (pH 6.0) for 10 min. Tissue sections were washed for 5 min in PBS with 0.1% Tween-20 (PBS-T), blocked at room temperature for 1 h with 3% bovine serum albumin in PBS-T, and then incubated with the primary antibody in a humidified chamber overnight at 4°C. After tissues were washed with PBS, sections were incubated with Alexa Fluor 546 and 488 conjugated secondary antibodies (Life Technologies) for 1 h at room temperature. Sections were washed with PBS-T and mounted with Prolong Gold Antifade mounting medium with DAPI (Invitrogen). Fluorescent images were viewed and captured using fluorescence microscopy, and all images were compiled using Photoshop CS4 or CS5 (Adobe Systems Inc.). TUNEL assay was performed as previously described [24], using a fluorescein in situ apoptosis kit (ApopTag; Millipore). TUNEL-positive cells were imaged using fluorescence microscopy and defined as apoptotic cells. The following antibodies were used in this study: goat anti-prostaglandin-endoperoxide synthase 2 (PTGS2; 1:200 dilution; Santa Cruz Biotechnology); rat anti-cytokeratin 8 (KRT8; Troma I; 1:200 dilution; Developmental Studies Hybridoma Bank); rabbit anti-alpha smooth muscle actin (α-SMA; 1:200 dilution; Abcam).

Statistical Analysis

Statistical analysis was performed using Prism 5 software (GraphPad) or SPSS statistics 22 (IBM). Multiple comparisons were performed using one-way ANOVA followed by Tukey honestly significant difference (HSD) post hoc test. Single comparisons were carried out using two-tailed, unpaired Student *t*-tests and a P value of <0.05 was considered statistically significant. Unless otherwise stated, results were obtained from at least three independent biological replicates and carried out in duplicate or triplicate technical replicates.

RESULTS

Triple Conditional Deletion of Smad1*,* Smad5*, and* Smad4 *using* Amhr2-cre *Results in Sterility*

We previously reported the fecundity of conditional deletions for *Smad1*, *Smad5*, *Smad4*, *Smad1/5*, and *Smad1/5/4* mouse models that used *Amhr2-cre* to delete the respectively floxed alleles [18, 27, 32]. A summary comparison of the fecundity of these models is given in Table 1. Single conditional deletion of *Smad1* or *Smad5* has no effect on female fertility [18, 23]. In contrast, conditional codeletion of *Smad1* and *Smad5* by using *Amhr2-cre* (*Smad1/5-Amhr2-cre* KO) causes reproductive defects and granulosa tumor development in female mice with full penetration. At younger ages (<4 mo old), female *Smad1/5-Amhr2-cre* KO mice are subfertile but are unable to produce litters after 4–6 mo of age concurrent with development of large

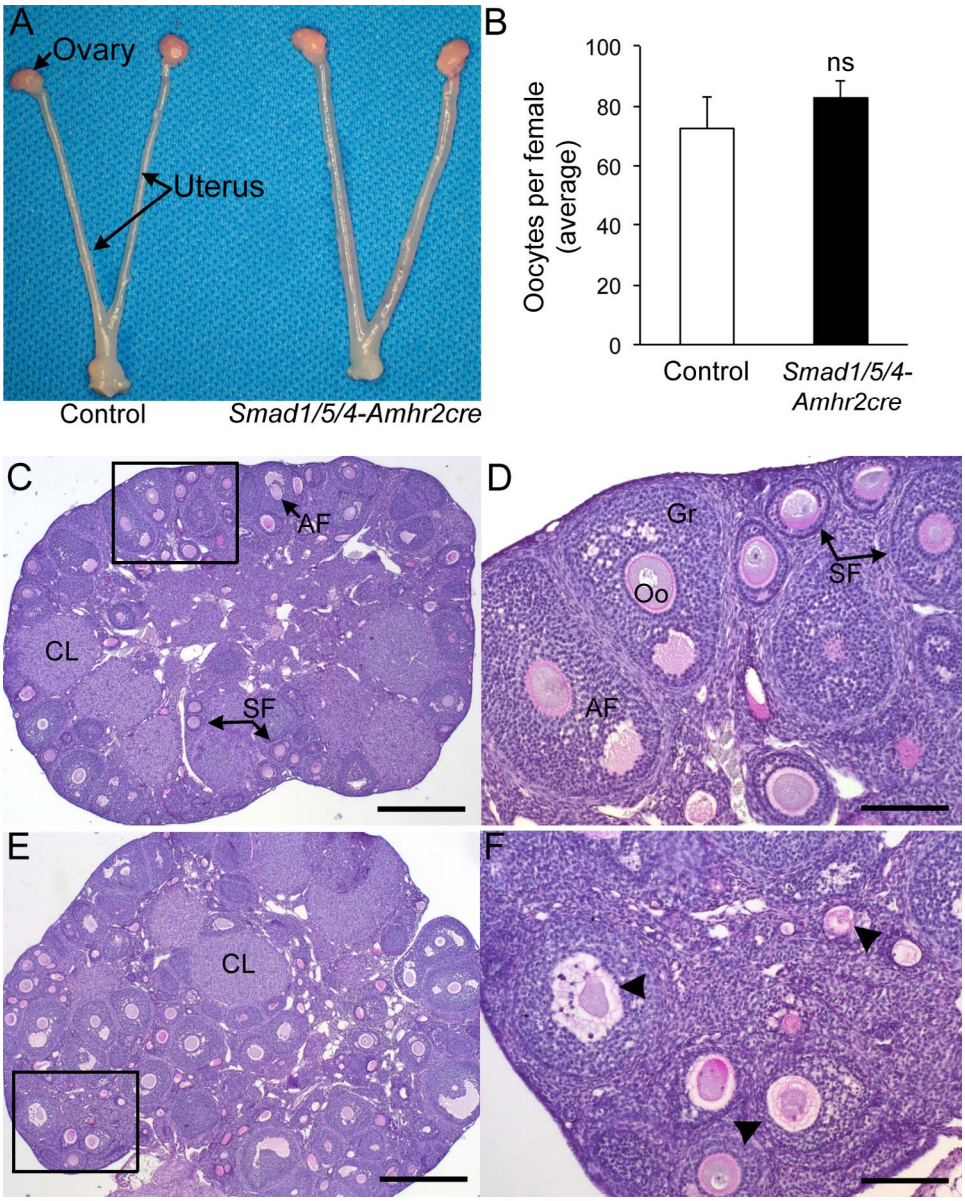

FIG. 1. Ovarian histology and ovulation in *Smad1/5/4-Amhr2-cre* KO female mice. **A**) Reproductive tract of *Smad1*$^{flox/flox}$ *Smad5*$^{flox/flox}$ *Smad4*$^{flox/flox}$ control (left) and *Smad1*$^{flox/flox}$ *Smad5*$^{flox/flox}$ *Smad4*$^{flox/flox}$ *Amhr2*$^{cre/+}$ KO mice at 6 wk of age. No gross differences were detected. **B**) Pharmacologic superovulation of control and *Smad1/5/4-Amhr2-cre* KO mice at 3 wk compared to control. No statistical differences (ns) were detected in the mean number of oocytes collected in the oviducts of control; n = 3 each genotype. **C**) PAS stain of an ovary from a 12-wk-old *Smad1*$^{flox/flox}$ *Smad5*$^{flox/flox}$ *Smad4*$^{flox/flox}$ control mouse shows normal follicular development with multiple corpora lutea (CL) and growing follicles (SF, secondary follicles; AF, antral follicle). **D**) Inset shown in panel **C** shown at 100x magnification. **E**) PAS stain of an ovary from a 12-wk-old *Smad1*$^{flox/flox}$ *Smad5*$^{flox/flox}$ *Smad4*$^{flox/flox}$ *Amhr2*$^{cre/+}$ KO female. All stages of follicles can be detected, including CLs. However, a large number of atretic follicles (arrowheads) are visible. **F**) Inset from panel **E** shown at 100x magnification. Previous quantification of the increased atretic follicles in the *Smad1/5/4-Amhr2-cre* KO mouse model has been published previously [24]. Bars = 200 μm (**C** and **E**) and 50 μm (**D** and **F**). Oo, oocyte; Gr, granulosa cell.

ovarian granulosa cell tumors [18] (Table 1). Young adult *Smad4-Amhr2-cre* KO mice are subfertile (Table 1), but by 4–6 mo of age, approximately half of the *Smad4-Amhr2-cre* KO females are infertile [27]. In contrast to these mouse models, we found that triple deletion of *Smad1*, *Smad5*, and *Smad4* (*Smad1/5/4-Amhr2-cre* KO) caused sterility (Table 1) [24]. Female *Smad1/5/4-Amhr2-cre* KO mice did not produce any litters in a 6-mo breeding trial that began at sexual maturity (6 wk of age) [32], but the cause of the infertility was unknown. Tumor development initiates in a similar time frame in *Smad1/5/4-Amhr2-cre* KO mice, but the tumors grow more slowly, do not metastasize, and have increased apoptosis [24]. Gross morphological examination of reproductive tracts from 6-wk-old female control and *Smad1/5/4-Amhr2-cre* KO mice appeared normal (Fig. 1A). In our initial characterization of the ovarian defects, we found a significant increase in the proportion of TUNEL-positive follicles in mutant ovaries [24]. However, even with the increased TUNEL-positive follicles, *Smad1/5/4-Amhr2-cre* KO ovaries contained follicles representing all follicular stages as well as corpora lutea (Fig. 1, C–F). The presence of corpora lutea suggested that despite their inability to produce live pups, *Smad1/5/4-Amhr2-cre* KO females were capable of ovulation (Fig. 1E). To test this, we pharmacologically ovulated sexually immature control (n = 3) and *Smad1/5/4-Amhr2-cre* KO females (n = 3) and collected oocytes from the ampulla of oviduct. We did not find statistical differences in the mean number of oocytes

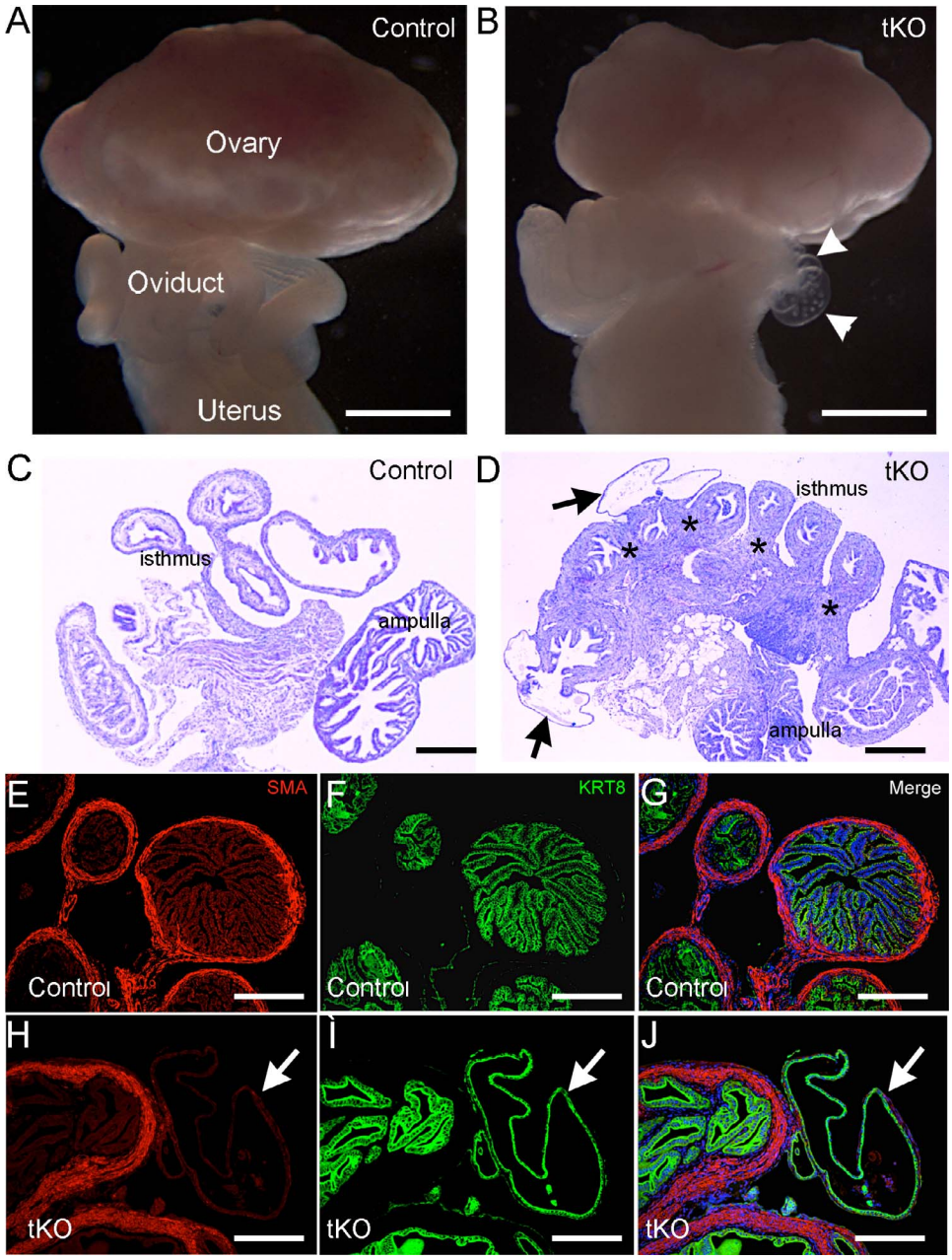

FIG. 2. Oviduct abnormalities in *Smad1/5/4-Amhr2-cre* KO mice. Gross morphology of reproductive tracts from 16-wk-old control mice (**A**) and 16-wk-old *Smad1/5/4-Amhr2-cre* KO (tKO) mice (**B**). *Smad1/5/4-Amhr2-cre* KO mice display oviduct diverticula, indicated in **B** (arrowheads). An enlarged image of the diverticuli is shown in Supplemental Figure S1. **C** and **D**) Histology of oviducts from 16-wk-old mice showing an increased oviduct thickness and oviduct diverticula (arrows) in *Smad1/5/4-Amhr2-cre* KOs (**D**) compared to control (**C**). **D**) *Abnormal regions of thickness. **E–J**) Immunofluorescence of smooth muscle actin (α-SMA) and cytokeratin 8 (KRT8) in the oviducts of 16-wk-old control (**E–G**) and *Smad1/5/4-Amhr2-cre* (**H–J**) mice. White arrowheads indicate KRT8^{+} oviduct diverticula in *Smad1/5/4-Amhr2-cre* KO mice (**H–J**) devoid of α-SMA immunoreactivity. Bars = 500 μm (**A** and **B**) and 200 μm (**C–J**).

ovulated between genotypes of immature mice (Fig. 1B). Thus, the ovarian defects (i.e., increased follicular atresia) are not likely to fully explain the sterility of young adult (6-wk-old) *Smad1/5/4-Amhr2-cre* KO females. Therefore, we additionally analyzed the reproductive tracts of these mice.

Amhr2-cre–*Mediated Deletion of* Smad1/5/4 *Results in Oviduct Abnormalities*

Apart from granulosa cells of growing follicles in the ovary, *Amhr2-cre* is known to express *Cre* recombinase in mesenchyme-derived tissues in the reproductive tract [25]. Deletion of genes such as *Dicer*, tuberous sclerosis 1 (*Tsc1*), and the TGFβ type I receptor gene *Tgfbr1* using *Amhr2-cre* leads to defects in oviduct development and uterine function [16, 33–35]. To examine the structural integrity of the reproductive tract and determine if any oviductal defect contributes to the sterility in *Smad1/5/4-Amhr2-cre* KO mice, we performed a morphological and histological analysis of adult *Smad1/5/4-Amhr2-cre* KO reproductive tracts. In mice at 16 wk of age, we found obvious development of clear fluid-filled bilateral oviductal diverticula throughout the length of each *Smad1/5/4-Amhr2-cre* KO oviduct in all of the mutant females examined (Fig. 2). Oviductal diverticuli were more abundant near the

uterotubal junction and often contained cellular debris and round structures that appeared to be oocytes or embryos (Fig. 2B, Supplemental Fig. S1). Neither *Smad4-Amhr2-cre* KO nor *Smad1/5-Amhr2-cre* KO females showed these diverticuli at any age (3 wk–1 yr old) (Table 1) [18, 27].

Histological examination of oviducts from 16-wk-old *Smad1/5/4-Amhr2-cre* KO mice revealed abnormalities in tissue morphology compared with controls. The stromal and muscle compartments were disorganized and had an abnormally thickened appearance in all oviduct regions of the *Smad1/5/4-Amhr2-cre* KO mice compared to those in control (Fig. 2, C and D, Supplemental Fig. S2). Often, histology specimens from random cycling female *Smad1/5/4-Amhr2-cre* KO mice showed oocytes/embryos within the lumen, which were only rarely seen in control samples (Supplemental Fig. S2). The thickened areas of the oviduct of *Smad1/5/4-Amhr2-cre* KO mice appeared to consist of mainly additional smooth muscle tissue, and many areas did not have the normal, clearly defined outer and inner smooth muscle layers (Fig. 2, D and H, Supplemental Fig. S2). Immunostaining of smooth muscle cell marker (α-smooth muscle actin [α-SMA]) demonstrated regions of increased thickness in smooth muscle layers within the oviductal ampulla (Fig. 2H). We also examined the epithelial cell marker KRT8; KRT8 staining demonstrated that oviductal diverticula in *Smad1/5/4-Amhr2-cre* KO oviducts were characterized by a single layer of flattened epithelium (Fig. 2, I and J, arrow), devoid of the smooth muscle layer.

For detailed volumetric structural analysis of the oviduct, we acquired 3D visualizations using OCT. Figure 3 shows representative cross-sections through the structural data sets of the oviduct acquired from 6-wk-old mice, prior to the development of large diverticuli. The mouse oviduct consists of four segments: the infundibulum, ampulla, isthmus, and uterotubal junction. The structure of the ampulla in *Smad1/5/4-Amhr2-cre* KO oviducts appeared normal. Specifically, the longitudinal epithelial folds in the *Smad1/5/4-Amhr2-cre* KO ampulla lumen exhibited patterns and density similar to those in controls (Fig. 3, A and B); the thickness of the ampulla wall and of the epithelial folds also appeared normal (Fig. 3, C and D). However, the isthmus of the *Smad1/5/4-Amhr2-cre* KO oviducts displayed an abnormal phenotype. Figure 3, E and F, shows surface views of the isthmus in controls and *Smad1/5/4-Amhr2-cre* KO oviducts. In contrast to the smooth appearance of the isthmus surface in control mice (Fig. 3E), the *Smad1/5/4-Amhr2-cre* KO oviducts appeared rough and uneven (Fig. 3F). Figure 3, G and H, shows corresponding semitransparent view of the same reconstruction. *Smad1/5/4-Amhr2-cre* KO mice displayed oviduct wall thickening, disorganized luminal folds, and a lack of transverse folding (Fig. 3H) in comparison to those of the control (Fig. 3G). However, the overall coiling pattern of the *Smad1/5/4-Amhr2-cre* KO oviducts appeared normal with some variation seen in both wild-type and *Smad1/5/4-Amhr2-cre* KO samples (Fig. 3, E–H).

To examine oviduct morphology after ovulation, we acquired OCT visualizations from pharmacologically ovulated 4-wk-old females 18 h after the ovulatory stimulus (injection of human chorionic gonadotropin) (Fig. 4). We observed the same defective appearance of the *Smad1/5/4-Amhr2-cre* KO oviduct coils at this stage although to a lower extent than at 6 wk of age, which is clearly visible in the surface rendering view of the data (Fig. 4, A and B). Semitransparent renderings of the OCT data sets show the smooth inner lumen of the oviduct in control mice (Fig. 4C) and disorganized lumen in *Smad1/5/4-Amhr2-cre* KO oviducts (Fig. 4D). Figure 4, E–H, shows structural analysis of the ampulla region. Semitransparent view (Fig. 4, E and F) shows similar epithelial folding patterns and COCs visible through the ampulla wall in control (Fig. 4E) and *Smad1/5/4-Amhr2-cre* (Fig. 4F) KO mice. In cross-sectional views of the same data sets, oocytes surrounded by cumulus cells are clearly visible in the ampulla of both the control and the *Smad1/5/4-Amhr2-cre* KO females; COCs appeared morphologically similar and went on to cumulus expansion in both genotypes (Fig. 4, G–J).

Loss of Smad1/5/4 *Leads to Altered Expression of Genes Essential for Oviduct Development and Differentiation*

The molecular processes of oviduct development and differentiation are poorly understood. Genetic deletion studies in mice implicate multiple developmental signaling pathways, such as the TGFβ [16], WNT/β-catenin [36], and micro-RNA biogenesis [33] pathways in oviduct formation. To examine whether loss of *Smad1/5/4* affected the gene expression pattern in the oviduct, we compared mRNA levels of candidate genes in 4- to 5-wk-old control oviducts with those in 4- to 5-wk-old *Smad1/5/4-Amhr2-cre* KO mice (Table 2). Of these genes, we observed significantly reduced mRNA levels of *Dicer* in *Smad1/5/4-Amhr2-cre* KO oviducts compared to those in controls. Similar to the molecular changes observed in *Dicer* conditional knockout (cKO) oviduct, we also found significant upregulation of wingless family member 5a (*Wnt5a)* and homeobox transcription factor 9 (*Hoxa9*). *Wnt5a* and the homeobox genes are known to play a pivotal role in patterning of the posterior Müllerian-derived structures [37–39]. However, mouse models with increased levels of *Wnt5a*, such as those with Müllerian duct mesenchymal stabilization of β-catenin (*Ctnnb1*) [40] or smoothened (*Smo*) [41] in the oviduct, displayed uncoiled oviducts and altered radial patterning, unlike the *Smad1/5/4-Amhr2-cre* KO line.

As *Amhr2* is expressed in the mesenchyme of the Müllerian duct, which gives rise to the smooth muscle of the oviduct and uterus, we further examined whether loss of *Smad1/5/4* affects the expression of genes important for smooth muscle development and differentiation (Table 2). *Smad1/5/4-Amhr2-cre* KO oviducts showed significantly increased expression of the smooth muscle markers desmin (*Des*) and transgelin (*Tagln*), the actin-linked regulatory protein calponin 1 (*Cnn1*), and the cytoskeleton protein smoothelin (*Smtn*). Caldesmon 1 (*Cald1*), a protein that interacts with actin, myosin, tropomyosin, and calmodulin, was also significantly upregulated in *Smad1/5/4-Amhr2-cre* KO oviducts compared to that in controls. Furthermore, the mRNA level of myocardin (*Myocd*), a smooth muscle and cardiac muscle-specific transcriptional coactivator and master regulator of smooth muscle contractile gene expression [42, 43] was increased in the *Smad1/5/4-Amhr2-cre* KO oviducts.

Loss of Smad1/5/4 *Disrupts Epithelium and Smooth Muscle Development in the Uterus*

The mouse uterus is composed of two major compartments, the endometrium and myometrium. The endometrial compartment consists of luminal and glandular epithelial cells as well as supporting stromal cells, whereas the myometrium consists of smooth muscle layers. Because the *Amhr2* promoter specifically directs expression of *Cre* recombinase in the stroma and myometrium but not in the epithelium, we next investigated the effect of *Smad1/5/4* loss in the uterus. We used co-immunostaining for α-SMA to delineate the muscle layers of the uterus [44] and KRT8 for the epithelium (Fig. 5). The control uteri showed two well-organized layers of longitudinal (outside) and circular (inside) smooth muscles (Fig. 5A, red).

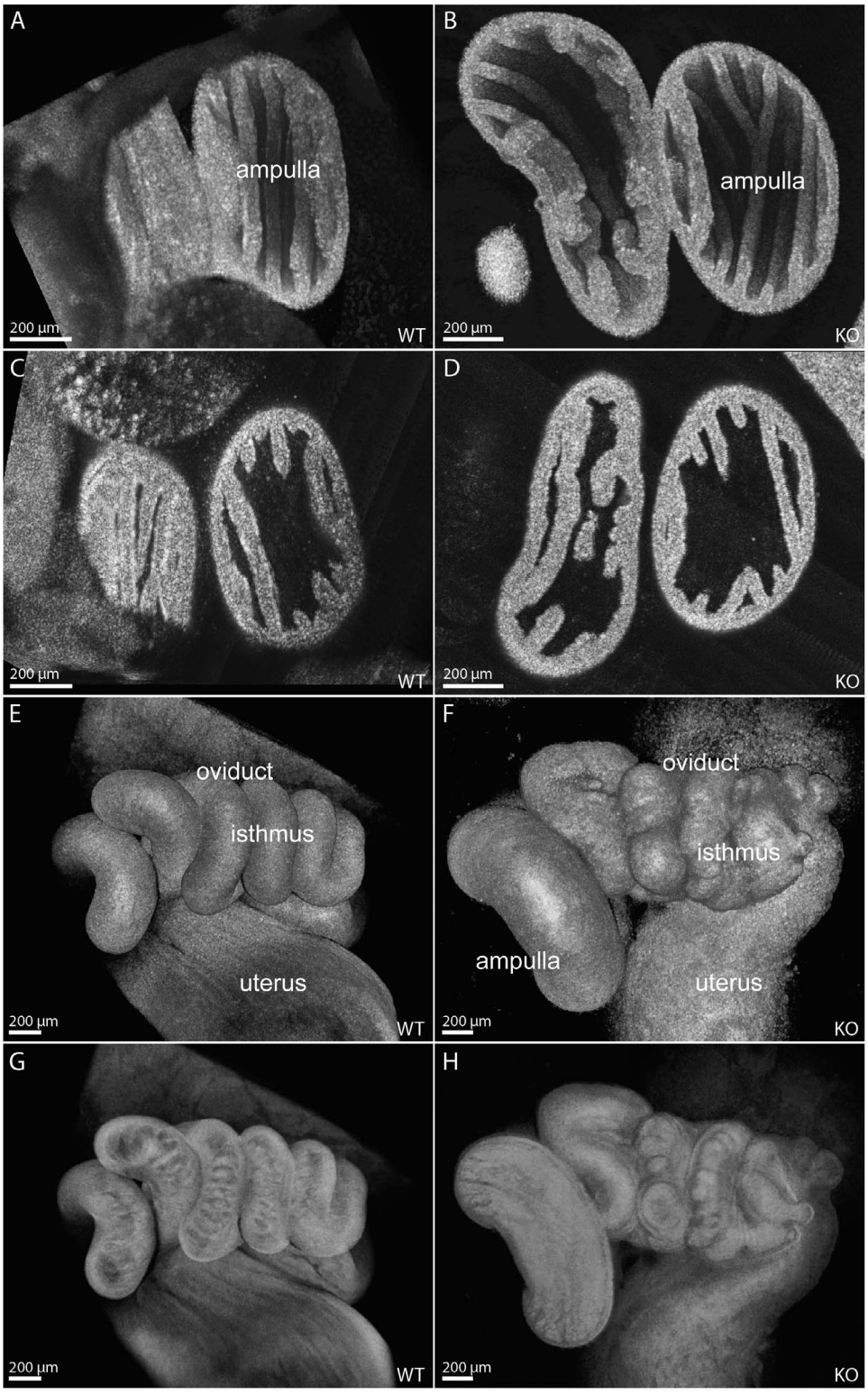

FIG. 3. Structural oviduct abnormalities in 6-wk-old *Smad1/5/4-Amhr2-cre* KO mice visualized with OCT. Three-dimensional reconstructions visualizing the luminal surface of control (**A**) and *Smad1/5/4-Amhr2-cre* KO (**B**) female oviduct ampulla display similar levels of epithelial folding and density. Cross-sectional views through the reconstructions show comparable ampulla wall thicknesses in control (**C**) and *Smad1/5/4-Amhr2-cre* KO (**D**) female oviducts. Surface renderings of volumetric reconstructions of control (**E**) and *Smad1/5/4-Amhr2-cre* KO (**F**) female oviduct isthmus show an abnormal, uneven surface in the mutant. Semitransparent renderings of the corresponding data sets reveal abnormal disorganized luminal folding structures in the isthmus of the mutants (**H**) in contrast to those in controls (**G**).

In contrast, the *Smad1/5/4-Amhr2-cre* KO showed a disorganized architecture with variable thickness and an indistinct boundary between the stromal and myometrial layers (Fig. 5B). In addition, in contrast to the simple columnar luminal epithelium of the control uterus (Fig. 5, A and C), the uteri of *Smad1/5/4-Amhr2-cre* KO female mice had a disrupted luminal epithelium with an irregular pattern of cells and, at times, a hyperplastic phenotype (Fig. 5, D and F). Epithelial

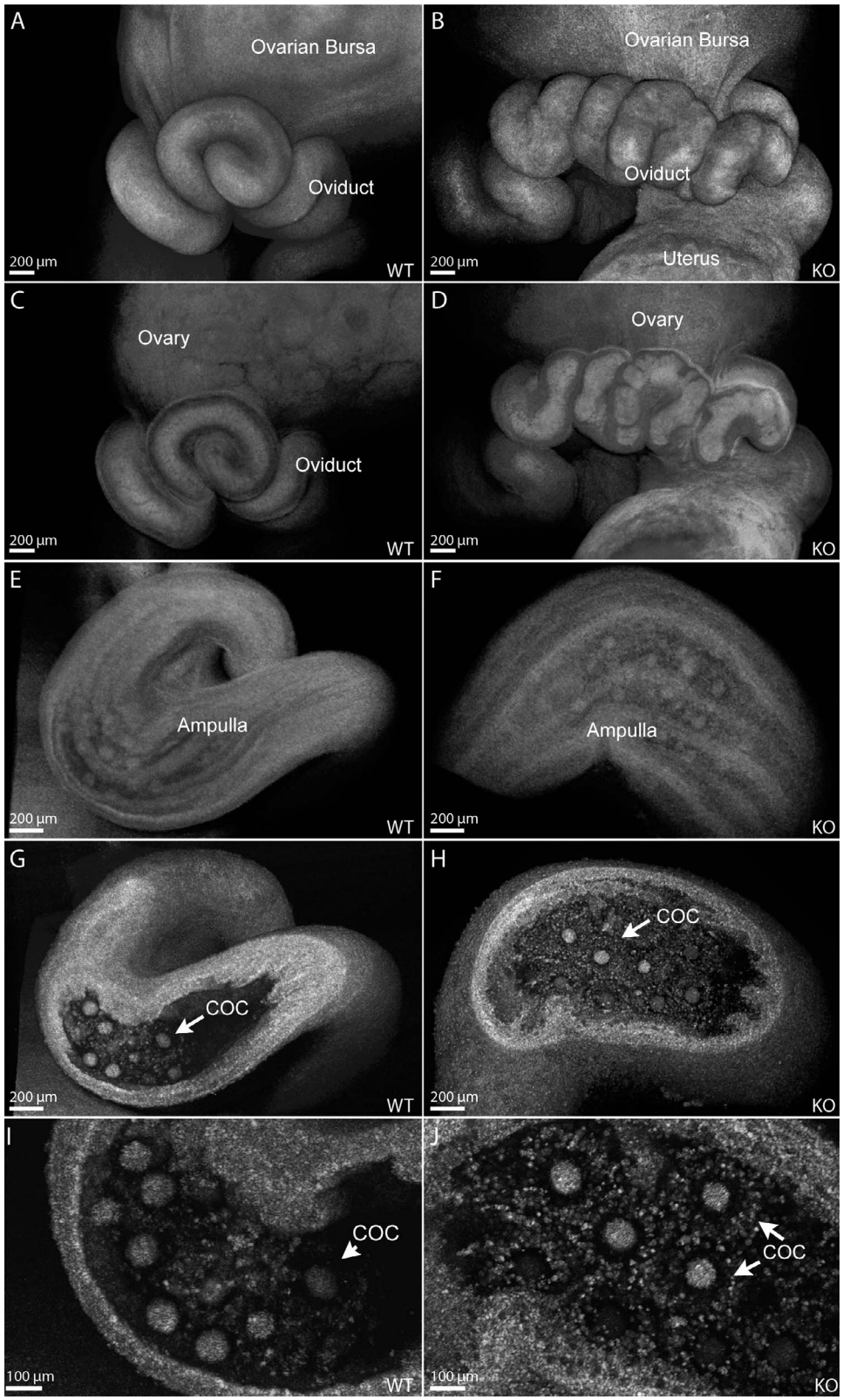

FIG. 4. Structural oviduct abnormalities in pharmacologically superovulated 4-wk-old *Smad1/5/4-Amhr2-cre* KO mice visualized with OCT. Surface renderings of volumetric reconstructions in control (**A**) and *Smad1/5/4-Amhr2-cre* KO (**B**) 4-wk-old female oviduct isthmus show an uneven appearance to a lower extent than at 6 wk of age. Semitransparent renderings demonstrate smooth luminal surfaces of the isthmus in control animals (**C**), which are disorganized in the mutants (**D**). Semitransparent renderings of the ampulla in control (**E**) and *Smad1/5/4-Amhr2-cre* KO (**F**) females show normal overall structure and longitudinal epithelial folding patterns. Cross-sectional views through the corresponding reconstructions reveal COCs in the ampulla of the mutants (**H**), which appeared similar to those in controls (**G**). Higher magnifications of **G** and **H** are shown in **I** and **J**, respectively. Scale bars are indicated in the left corner of each panel.

TABLE 2. Gene expression changes in *Smad1/5/4-Amhr2-cre* KO oviducts.*

Gene	Description	Fold change†
Smooth muscle markers		
Des	Desmin	+2.60[a]
Cnn1	Calponin 1	+1.92[a]
Smtn	Smoothelin	+1.91[a]
Tagln	Transgelin	+1.51[b]
Cald1	Caldesmon 1	+1.25[b]
Myocd	Myocardin	+1.65[b]
Acta2	Actin, alpha 2, smooth muscle, aorta	NS
Myh11	Myosin, heavy polypeptide 11, smooth muscle	NS
Wnt ligands		
Wnt5a	Wingless-related MMTV integration site family member 5a‡	+1.57[a]
Wnt7a	Wingless-related MMTV integration site family member 7a‡	NS
MicroRNA pathway		
Dicer	Dicer 1, ribonuclease type III	−0.60[a]
Homeobox transcription factor		
Hoxa9	Homeobox A9	+1.44[b]

* Summary of qPCR gene expression results from 12-wk-old control and *Smad1/5/4-Amhr2-cre* KO oviducts. RNA was normalized to *Gapdh* levels.
† Fold change values are relative to control ($Smad1^{flox/flox}$ $Smad5^{flox/flox}$ $Smad4^{flox/flox}$). NS, not significantly different from controls.
‡ MMTV, Mouse mammary tumor virus.
[a] $P < 0.001$; [b] $P < 0.05$ by Student *t*-test between genotypes.

cells also showed a high degree of apoptosis, as indicated by histology and TUNEL assay (Fig. 5, F and H).

Loss of Smad1/5/4 *Causes Defective Implantation and Loss of Embryos During Pregnancy*

Because the endometrial stromal component of the uterus is derived from *Amhr2*-expressing Müllerian duct mesenchyme, we next investigated whether loss of *Smad1/5/4* in endometrial stroma could lead to defective implantation. Successful implantation requires a series of well-coordinated physical-physiological interactions among the blastocyst and the trophectoderm and various endometrial cell types, including the luminal and glandular epithelium and stromal cells. In mice, the process of implantation is initiated by blastocyst attachment to the uterine luminal epithelium, which occurs on Days 4–5 of pregnancy. To ascertain the stage-specific failure of pregnancy, 8-wk-old control and *Smad1/5/4-Amhr2-cre* KO females were mated with wild-type males, and natural pregnancy was examined on different embryonic days. Fewer implantation sites were found at E4.5, E5.5, and E7.5 (Fig. 6, A, B, D, and E, Supplemental Figs. S3 and S4), which also appeared smaller in size (Fig. 6, A, B, D, and E, Supplemental Fig. S4). By E9.5, no implantations could be detected in any *Smad1/5/4-Amhr2-cre* KO uterus (Fig. 6, C and F).

To further characterize the reason for pregnancy failure, we collected uteri from pregnant females at E5.5 and E7.5 and examined the histology of the implantation sites. Control mice exhibited well-attached embryos and induction of a decidual response at E5.5 (Supplemental Fig. S4, A and B). Unlike control mice at E5.5, we observed that *Smad1/5/4-Amhr2-cre* KO mice failed to assemble a closed uterine lumen, which is essential for successful embryo attachment and critical for establishing intimate contact of the blastocyst and the uterine epithelium that is required for embryo survival (Supplemental Fig. S4, A and B). In control mice by E7.5, the lumen was not visible, and the luminal epithelium had undergone regression (Fig. 6I). In the *Smad1/5/4-Amhr2-cre* KO, the lumen remained open, and the luminal epithelium was still apparent as a single, organized layer (Fig. 6, G–J). These results suggested that *Smad1/5/4-Amhr2-cre* KO mice have defects in pregnancy that may be caused, in part, by the failure of closure of the uterine lumen.

Amhr2-cre–*Mediated Deletion of* Smad1/5/4 *in Uterus Compromises Decidualization and* Ptgs2 *Expression*

In response to implantation, stromal cells surrounding the implanting embryo undergo extensive proliferation and subsequent differentiation into polyploid decidual cells in a process termed decidualization [4]. Several studies provided direct evidence that a fully developed decidua is mandatory for providing nutrition to the developing embryo and acting as a barrier that prevents uncontrolled trophoblast invasion and protecting the embryo from maternal rejection prior to the formation of functional placenta [4]. We examined decidualization in timed-mated pregnancies by isolating maternal decidua from E6.5 implantation sites in *Smad1/5/4-Amhr2-cre* KO and control uteri. In *Smad1/5/4-Amhr2-cre* KO mice, the stroma appeared to only partially decidualize around implanted embryos in comparison to control embryos (Supplemental Fig. S4, C and D). We therefore tested whether *Smad1/5/4-Amhr2-cre* KO mice were able to undergo decidualization in a well-characterized artificial decidualization assay [28]. Ovariectomized control and *Smad1/5/4-Amhr2-cre* KO mice were treated with E2 and P4 to induce receptivity and synchronize the estrous cycle. Embryo implantation was mimicked by physically traumatizing the entire length of uterine endometrium of the left uterine horn. The right horn was left unstimulated as a control. Consistent with the reduced size of implantation sites during natural pregnancy, we observed that *Smad1/5/4-Amhr2-cre* KO females failed to respond to the decidual stimulus 2 days after the trauma compared to control littermates (Fig. 7A). At 4 days, the difference in size of the stimulated to unstimulated horn of *Smad1/5/4-Amhr2-cre* KO mice to control mice was even greater (Fig. 7B). A quantification of the decidual response by measurement of uterine wet weight showed the stimulated horn of the *Smad1/5/4-Amhr2-cre* KO mice failed to increase in size in comparison to that in littermate controls (Fig. 7C). Furthermore, we examined alkaline phosphatase activity to assess stromal cell differentiation during decidualization [45]. Compared to controls, which had robust alkaline phosphatase staining, the *Smad1/5/4-Amhr2-cre* KO showed no reaction (Supplemental Fig. S5). These results confirm that, even when injected with appropriate hormones and given an initiating decidual cue, the uteri of *Smad1/5/4-Amhr2-cre* KO mice are not able to appropriately decidualize.

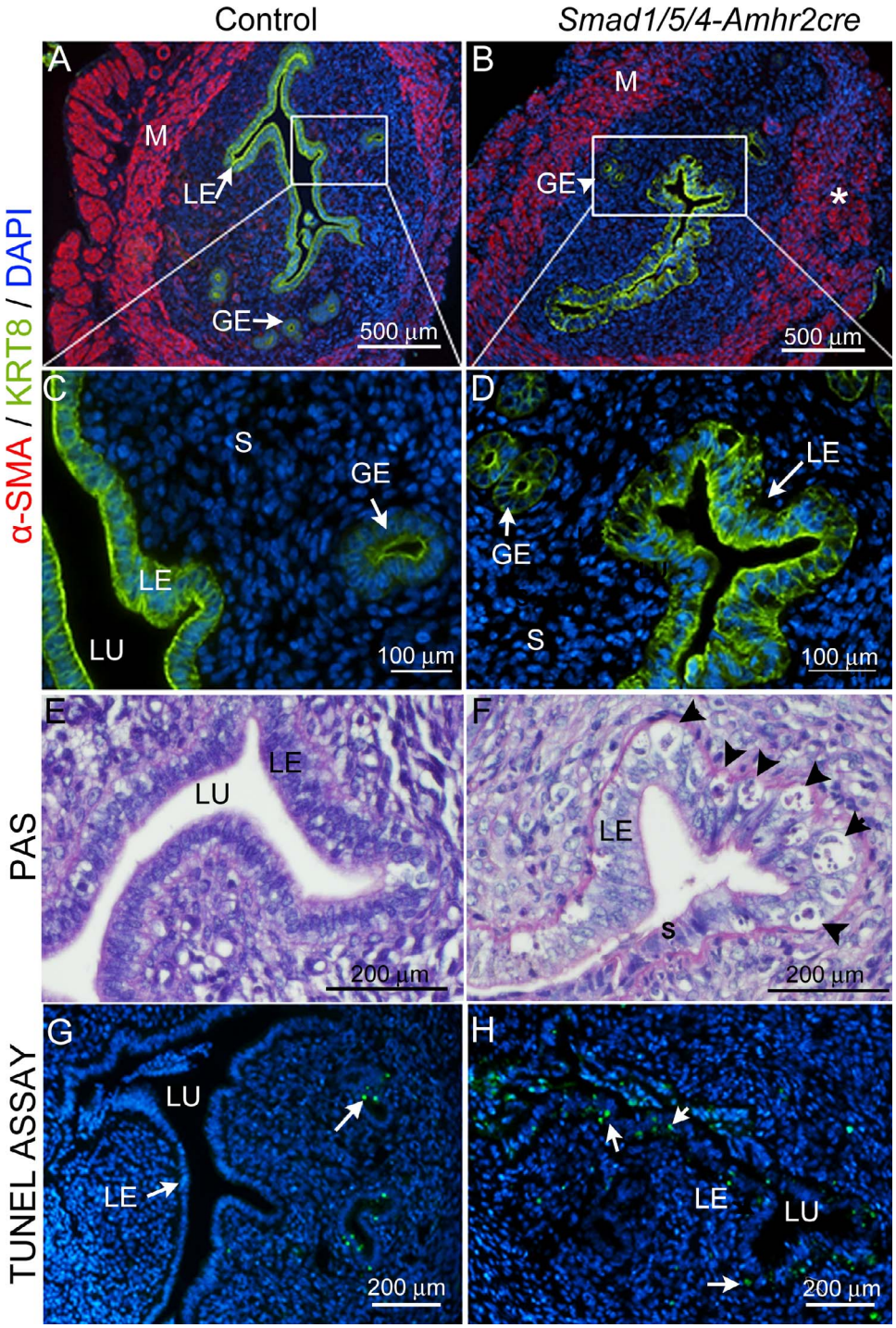

FIG. 5. Loss of *Smad1/5/4* disrupted smooth muscle development in uterus is shown and causes epithelial hyperplasia and apoptosis. Immunostaining of control (**A** and **C**) and *Smad1/5/4-Amhr2-cre* KO (**B** and **D**) in 6-wk-old uterus with the myometrium marker α-SMA (red) and the epithelial marker KRT8 (green). Insets in **A** and **B** are shown at 160X magnification for the luminal epithelium in **C** (control) and **D** (*Smad1/5/4-Amhr2-cre* KO). Compared to those in control, *Smad1/5/4-Amhr2-cre* KO uteri have disorganized myometrium (**B***) and large vacuolated apoptotic cells in luminal epithelium (**D** and **F**). Six-wk-old sections of uteri were stained with PAS to show the histology of the uterine epithelium in control (**E**) and *Smad1/5/4-Amhr2-cre* knockout (**F**) mice. Vacuolated apoptotic cells in the luminal epithelium are indicated by arrowheads in **F**. **G** and **H**) TUNEL analysis for apoptotic cells (green) in uteri of 6-wk-old control (**G**) and *Smad1/5/4-Amhr2-cre* (**H**) KO mice. Nuclei are counterstained with DAPI (blue). Arrows indicate TUNEL-positive cells (green). GE, glandular epithelium; LE, luminal epithelium; M, myometrium; S, stroma; LU, lumen.

Because of defects in both the natural and artificial decidualization experiments, we analyzed expression of a number of key decidual markers in total RNA extracts prepared from decidua collected at E6.5 from natural pregnancies (Table 3). We did not observe significant changes in expression of cyclin E2 (*Ccne2*), FK506 binding protein 5 (*Fkbp5*), estrogen receptor alpha (*Esr1*), or *Pgr*, genes known to change expression during decidualization. In contrast, we found significantly decreased expression of *Bmp2* and *Wnt4*, two well-known markers whose expression is greatly induced upon

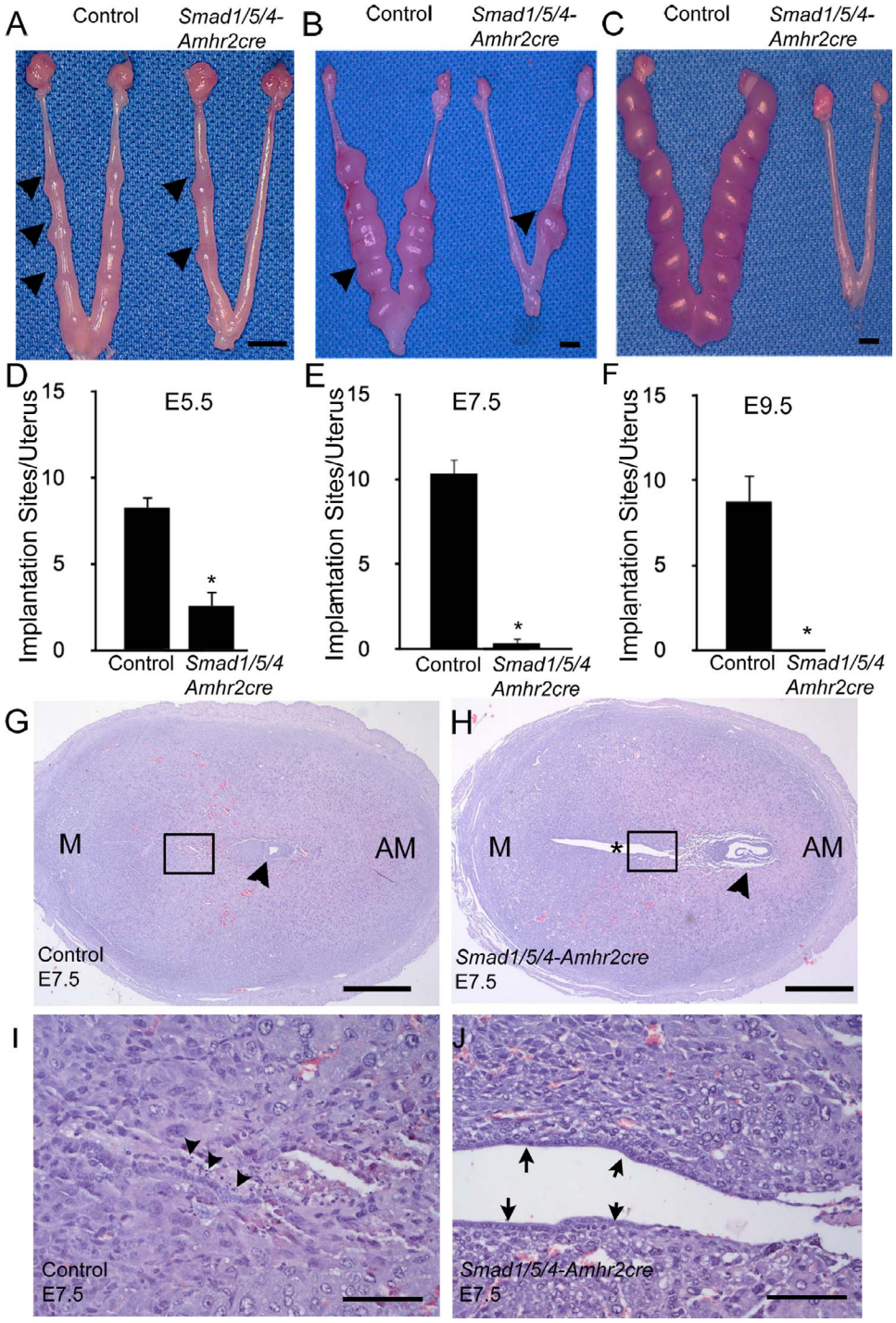

FIG. 6. *Smad1/5/4-Amhr2-cre* mutants have implantation failure and defective embryo attachment. **A**–**F**) Mice were euthanized at E5.5, E7.5, and E9.5, and the numbers of implantation sites were counted in control and *Smad1/5/4-Amhr2-cre* KO mice. Arrowheads indicate implantation sites. Data are represented as means ± SEM; at least 3 mice were analyzed per genotype. Two-tailed unpaired Student *t* test was used to compare the control and *Smad1/5/4-Amhr2-cre* KO mice (*$P < 0.05$). **G** and **H**) H&E staining of control and *Smad1/5/4-Amhr2-cre* KO implantation sites at E7.5. **G**) Control embryo (arrowhead) with well-closed lumen and differentiated surrounding stroma. Insets from **G** and **H** are shown in **I** and **J**, respectively. **H**) *Smad1/5/4-Amhr2-cre* KO embryo (arrowhead) appeared to be degenerating, the uterus showed an *open lumen, and stromal cells have not fully differentiated. **I** and **J**) 125x magnification of insets shown in **G** and **H**, respectively. The luminal epithelium in control uteri has fully closed, and cells show signs of apoptosis (arrowheads). **J**). The luminal epithelium in knockout uteri remains visible (arrows). Bars = 5 mm (**A–C**), 400 μm (**G** and **H**), and 100 μm (**I** and **J**).

decidualization. We also found a significant reduction in *Ptgs2*, a marker of implantation and decidualization. Immunofluorescence analysis of PTGS2 demonstrated a reduction in immunoreactivity in *Smad1/5/4-Amhr2-cre* KO decidual cells at the mesometrial pole at E5.5 in KO mice compared to that in the controls (Fig. 7, D–G). These data indicated that *Smad1/5/4-Amhr2-cre* KO uteri were unable to undergo normal decidualization at least in part due to decreased expression of known regulators of decidualization including *Bmp2*, *Wnt4*, and *Ptgs2*.

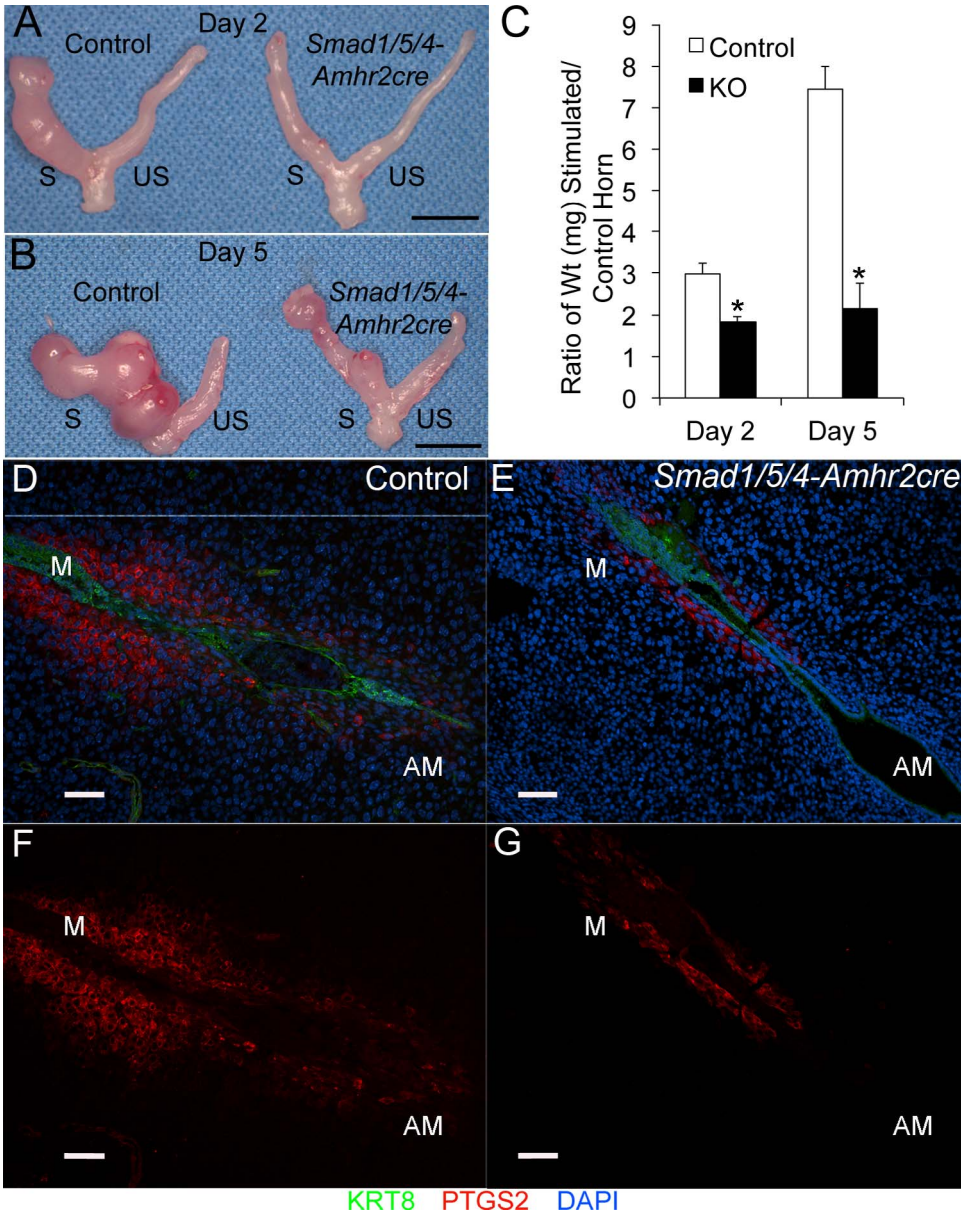

FIG. 7. *Smad1/5/4-Amhr2-cre* KO mice show defective decidualization and loss of PTGS2. **A–C**) Uterine decidualization was artificially induced in hormone-stimulated ovariectomized females by traumatizing the antimesometrial luminal epithelium with a needle in control and *Smad1/5/4-Amhr2-cre* KO uteri. Day 2 (**A**) and Day 5 (**B**) uteri collected after the trauma are shown. The stimulated horn is labeled S, and the unstimulated horn is labeled US. **C**) Ratio of uterine wet weight of stimulated to unstimulated horns collected 2 days and 5 days after the trauma. *Smad1/5/4-Amhr2-cre* KO females (Day 2, n = 3; Day 5, n = 4) did not show a response to the decidual stimulus compared to controls (Day 2, n = 3; Day 5, n = 3). *Statistical significance, $P < 0.05$. **D–G**) *Smad1/5/4-Amhr2-cre* KO females demonstrate loss of PTGS2 production during decidualization in natural pregnancies. Immunoreactivity of PTGS2 and KRT8 were determined by immunofluorescence analysis at E5.5. *Smad1/5/4-Amhr2-cre* mutants (**E** and **G**) display decreased PTGS2 (**D** and **F**) in the decidual cells at the mesometrial pole compared to control mice (**A** and **C**). Bars = 1 cm (**A** and **B**) and 100 μm (**D–G**). AM, antimesometrium; M, mesometrium.

DISCUSSION

The SMAD transcription factors play key developmental and homeostatic roles in multiple tissues. We analyzed the function of the receptor-regulated SMADs SMAD1 and SMAD5, which signal downstream of multiple TGFβ superfamily type I receptors (*Alk1*, *Alk2*, *Alk3*, *Alk6*, *Alk7*) and their trimerization partner SMAD4, using the well-characterized *Amhr2-cre* mouse model [26]. The *Amhr2-cre*, a knock-in of *Cre* recombinase into the *Amhr2* locus, deletes the *loxP*-flanked *Smad* genes in multiple tissues, including the ovary, oviduct, and uterus, and has been a well-established model for deletion in the granulosa cells of the ovary and mesenchymal derivatives of the Müllerian duct that give rise to the cells of the smooth muscle layers of the oviduct and uterus and the uterine endometrial stroma [16, 18, 24, 26, 33, 46, 47]. A number of studies have defined roles for the TGFβ superfamily receptors *Bmpr2*, *Alk2*, *Alk3*, *Alk4*, and *Alk5* during pregnancy by generating cKOs in the uterine epithelium by using *Pgr-cre* [14, 15, 48–50]. To our knowledge, this is the first cKO for any *Smad* gene to show a phenotype in the uterus or the oviduct. We previously used the triple *Smad1/5/4-Amhr2-cre* KO mutant mouse model to compare the phenotypic differences in the double *Smad1/5-Amhr2-cre* KO mutant mice on granulosa cell tumor development and showed that loss of

TABLE 3. Gene expression changes in *Smad1/5/4-Amhr2-cre* KO decidua collected at E6.5.[a]

Gene	Description	Fold change[b]
Bmp2	Bone morphogenetic protein 2	−2.14*
Ccne2	Cyclin E2	NS
Esr-1	Estrogen receptor 1	NS
Fkbp5	FK506 binding protein 5	NS
Gja1	Gap junction protein, alpha 1	NS
Lefty	Left right determination factor	NS
Mcm5	Mini chromosome maintenance complex component-5	−1.76*
Prl8a2	Prolactin family 8, subfamily a, member 2	NS
Pgr	Progesterone receptor	NS
Ptgs2	Prostaglandin-endoperoxide synthase 2	−1.91*
Wnt4	Wingless type MMTV integration site family member 4	−2.18*

[a] qPCR analysis compares gene expression between control (n = 4) and *Smad1/5/4-Amhr2-cre* KO (n = 3) decidua collected at E6.5. *Rpl19* was used as a housekeeping gene to normalize samples.
[b] Fold change values are relative to control littermates (*Smad1*$^{flox/flox}$ *Smad5*$^{flox/flox}$ *Smad4*$^{flox/flox}$). NS = not significant.
* $P < 0.05$ by Student *t*-test between genotypes.

Smad4 from *Smad1/5-Amhr2-cre* limits granulosa cell tumor progression and metastasis by increasing granulosa cell and tumor cell apoptosis [24]. In this study, we determined the uncharacterized effects of *Smad1/5/4* deletion on female fertility and the female reproductive tract. Unlike the single or double conditional KOs (Table 1), the triple cKO of *Smad1/5/4-Amhr2-cre* demonstrated sterility and severe developmental defects in the oviduct and uterus. The oviduct defects included disrupted organization and local expansion of the smooth muscle layers of the oviduct, which could lead to impaired oviduct muscular contractions and contribute to the embryo retention phenotype seen in the diverticula, similar to other mouse models [51]. There are also defects found in the uterine smooth muscle development and luminal epithelium of nonpregnant *Smad1/5/4-Amhr2-cre* KO females, including epithelial hyperplasia. Because *Amhr2-cre* does not express Cre recombinase in the uterine epithelium, the hyperplasia likely resulted from abnormal paracrine signaling from the uterine stroma, where Cre recombinase is expressed [25, 26]. This hyperplasia may additionally disrupt attachment of the blastocyst during implantation, further contributing to the sterility of the *Smad1/5/4-Amhr2-cre* KO females. Only a small number of embryos were found in *Smad1/5/4-Amhr2-cre* KO uteri at E4.5 and E5.5, but no implantations sites were found past mid-gestation. This may be due to a variety of factors in different tissues. First, the embryo quality may be poor perhaps due to improper oocyte development within the *Smad1/5/4-Amhr2-cre* KO follicles. Second, the environment of the oviduct may disrupt the timing or quality of development. Third, there is incomplete uterine closure and defective decidualization through loss of key factors, including *Bmp2*, *Wnt4*, and *Ptgs2*. Thus, there is probably not a primary defect but compound defects in multiple tissues that lead to the sterility in *Smad1/5/4-Amhr2-cre* KO females.

In this study, we pioneered the application of OCT for structural phenotyping of the oviduct in mouse mutants. This noninvasive 3D optical imaging technique is based on analysis of interferometry and provides a resolution of approximately 2–10 μm (less than the size of a cell) at a depth of a few millimeters. Because OCT relies on natural tissue contrast and does not require application of contrast agents, it is compatible with live imaging as performed in our study. Recently, we developed methods for structural analysis of mouse reproductive organs in vitro and in vivo and demonstrated that this method can be used for high-resolution volumetric visualization of the reproductive tract, oviduct lumen, and preimplantation embryos as well as for functional analysis of cilia dynamics [52–54]. Using this technique, we were able to clearly visualize the full extent of the defective development of the *Smad1/5/4-Amhr2-cre* KO model that was not immediately obvious by gross examination or by standard histology. The coiled isthmus at 3 wk of age displayed a rough surface and a disorganized epithelium but no large diverticuli. This phenotype was more severe at 6 wk of age, with a large number of bulges and pockets throughout the isthmus and a highly disorganized lumen. In contrast to luminal longitudinal folds wrapped in a thin layer of smooth muscle as seen in the ampulla, the folding pattern in the healthy isthmus transitions to nodules of folded epithelium arranged in longitudinal rows in the anterior isthmus, followed by ring-like transverse folds in the posterior isthmus and is surrounded by a much thicker smooth muscle layer. These folding patterns are disrupted in the mutant isthmus. The phenotype is more pronounced in the isthmus than the ampulla, possibly due to the known increased smooth muscle content of the isthmus compared to the ampulla. To the best of our knowledge, this is the first time OCT imaging has been implemented for structural phenotyping of the female reproductive tract in a novel mouse mutant. It provides valuable volumetric structural information, which is not accessible through histological analysis or other routinely used imaging methods in reproductive research. OCT imaging has the benefit of being a fast, noninvasive method that does not require any contrast agents or vital reporters and is compatible with live imaging. These features make this imaging approach a unique phenotyping tool for structural defects of reproductive organs with potential for longitudinal studies. Thus OCT will be of added benefit to investigators studying multiple aspects of the ovary and reproductive tract.

A previous mouse model that deleted the TGFβ type I receptor, *Tgfbr1*, using *Amhr2-cre* also has a sterility phenotype with defects in the oviduct and uterus, as outlined in Table 4. Surprisingly, neither the *Smad4-Amhr2-cre* KO nor the *Smad2/3-Amhr2-cre* KO mouse model has been reported to show these defects [22, 27]. Adult (16-wk-old) *Smad1/5/4-Amhr2-cre* KO oviducts also developed diverticuli within the oviduct, although unlike other models (Table 4), there was no evidence of overtly large oviductal diverticuli at 3–6 wk of age by histology or by OCT analysis. This would suggest that the oviductal diverticuli are not the primary cause of the sterility in younger *Smad1/5/4-Amhr2-cre* KO females. Despite the occurrence of an oviductal diverticuli phenotype in these three mouse models, there are distinct differences between them, including in gene expression changes and effects on the smooth muscle layers (Table 4). Loss of *Smad1*, *Smad5*, and *Smad4* should limit all TGFβ superfamily signaling that requires SMAD4 as well as abrogate signaling that is dependent upon

TABLE 4. Summary of phenotypes of *Amhr2-cre* mouse models that develop oviduct diverticuli.*

Parameter	*Dicer-Amhr2-cre*	*Tgfbr1-Amhr2-cre*	*Smad1/5/4-Amhr2-cre*
Ovary			
Fertility	Sterile	Sterile	Sterile
Follicle atresia	Increased	Normal	Increased
Ovulation†	Fewer eggs	Fewer eggs	No change
Oviduct			
Gross size	Reduced	ND	Thickened
Coiling	Reduced	Normal	Normal
Smooth muscle	Normal	Decreased	Increased
Inflammation	Present	ND	ND
Diverticuli	Yes, early (3–4 wk)	Yes, early (3 wk)	Yes, late (3–4 mo)
Uterus			
Gross size	Shorter	No change	No change
Glands	Fewer	ND	ND
Myometrium	Normal	Disorganized	Disorganized
Epithelium	Normal	ND	Hyperplastic
Decidual response	Normal	Normal	Reduced
Gene expression			
Myocd	ND	Reduced	Increased
Acta1	ND	Reduced	ND
Cnn1	Reduced	Reduced	Increased
Tagln	Increased	Reduced	Increased
Smtn	Increased	Reduced	Increased
Myh11	Increased	Reduced	Increased
Des	Increased	Reduced	Increased

* Description is the change in the mutant relative to its control. ND, not determined. Original descriptions of the phenotypes are provided in *Dicer-Amhr2-cre* [33], *Tgfbr1-Amhr2-cre* [16], and *Smad1/5/4-Amhr2-cre* [24].
† Ovulation was pharmacologically induced in sexually immature mice.

SMAD1 and SMAD5, such as that for the BMPs. Because loss of *Smad1*/*5*, loss of *Smad2*/*3*, or loss of *Smad4* alone does not have visible or obvious defects in oviductal or uterine smooth muscle layers, it is possible that multiple SMAD pathways may be redundant with respect to its development.

Embryo transit through the oviduct requires at least three related mechanisms, including ciliary motion, muscle contraction, and tubal fluid. The most obvious histologic defect in the *Smad1*/*5*/*4-Amhr2-cre* KO oviduct was disrupted development of the muscle layer, the myosalpinx. Little is known about the molecular mechanisms that control smooth muscle layer development of the oviduct, but both the myosalpinx and the myometrium appear to differentiate after birth [55–57]. In the oviduct, the myosalpinx varies in thickness, thicker in the oviduct isthmus than the ampulla [55]. In the *Smad1*/*5*/*4-Amhr2-cre* KO oviduct, the smooth muscle layer appeared thickened, particularly in the oviduct isthmus, and *Smad1*/*5*/*4-Amhr2-cre* KO oviduct samples abnormally overexpressed a number of smooth muscle markers, such as *Des*, *Tagln*, and *Myocd*. Thus, loss of SMAD signaling may increase the number of smooth muscle cells, as indicated by the increase in *Myocd* expression and/or their disorganized growth. However, *Smad1*/*5*/*4-Amhr2-cre* KO females did not develop uterine tumors, even though some of the KOs were housed for well over a year [24]. The changes to the smooth muscle layer prior to overt diverticuli formation could alter the kinetics of oocyte/embryo transit and contribute to the sterility phenotype of the *Smad1*/*5*/*4-Amhr2-cre* KO mouse. In support of this, we often found oocytes within most histologic specimens of the *Smad1*/*5*/*4-Amhr2-cre* KO oviduct, in contrast to the control. Thus, the *Smad1*/*5*/*4-Amhr2-cre* KO mutant mouse model would be an excellent model for future functional experiments to determine how structural alterations in the muscle layer of the oviduct can specifically affect oocyte, embryo, or sperm transit through the oviduct and potentially impact fertilization. In addition, it would be interesting to determine if the changes in stromal cells will alter epithelial cell function, for instance, possibly affecting ciliary beating.

While the reduction in the number of implantation sites at E5.5 may be a result of improper transit through the oviducts due to defective structure of the oviductal smooth muscle layer, some embryos clearly transit the oviduct but fail to develop normally as all implantation sites are fully lost by E9.5. Both implantation and decidualization appear to be affected by the loss of *Smad1*/*5*/*4*. During implantation, in a process called apposition, the embryonic trophectoderm becomes closely juxtaposed to the luminal epithelium, followed by closure of the uterine lumen. In the *Smad1*/*5*/*4-Amhr2-cre* KO implantation sites, the lumen only partially closes. This may be due to loss of *Ptgs2* expression in decidualizing cells at the mesometrial pole of implantation sites during early pregnancy (E5.5). Furthermore, we found that gene expression of *Bmp2* and *Wnt4*, key regulators of decidualization, were significantly decreased in *Smad1*/*5*/*4-Amhr2cre* KO females (E6.5). Previous studies using an in vitro decidualization system imply that BMP2-mediated SMAD1/5/8 signaling is important for the differentiation of stromal cells into decidual cells during pregnancy in mice and humans [58, 59]. Multiple KO mouse models have also established that *Bmp2* induces expression of both *Wnt4* and *Ptgs2* during decidualization [13, 60]. Thus, loss of *Bmp2* appears to be one of the primary causes of the uterine decidualization defect. Interestingly, although decidualization is a largely progesterone (P4)-dependent process, the decrease in expression of *Bmp2* in *Smad1*/*5*/*4-Amhr2-cre* KO females does not appear to be due to loss in expression of *Pgr*, as *Pgr* and other PGR target genes, such as *Fkbp5*, are normally expressed. Furthermore, decidualization cannot proceed in the *Smad1*/*5*/*4-Amhr2-cre* KO uteri even during artificial decidualization assays when P4 is exogenously supplied. This may mean that SMAD1/5/4 signaling is required for stromal upregulation of *Bmp2*, possibly as cofactors in conjunction with PGR signaling for a subset of genes. Other studies have demonstrated that loss of TGF-β signaling using

PGR-*cre* results in defective luminal closure as well as altered PTGS2 expression during peri-implantation [50]. Our mouse model provides further support that both BMP and TGF-β signaling pathways through the common transducer *Smad4*, are key pathways in stromal cells for uterine decidualization and pregnancy.

In summary, the present study provides the first genetic evidence that *Smad1/5/4*-mediated signaling is indispensable for structural and functional integrity of the oviduct and uterus. Loss of *Smad1/5/4* alters development of the oviduct smooth muscle layer, which likely impedes embryo transit. Disruption of SMAD-mediated signaling also alters development of the myometrium and defects in the uterine stroma leading to early pregnancy loss due to abnormal uterine structure, defective decidualization, and dysregulation of genes of known importance in oviduct development and uterine biology. We provided evidence to support the possibility that the SMAD signaling pathways may control early molecular and cellular changes in the uterus that are required for implantation and decidualization. We also showed that oviduct integrity also involves SMAD signaling in the myosalpinx. An in-depth knowledge of the molecular mechanisms and signaling networks involved in the regulation of early pregnancy events such as these has potential implications in developing new therapies for improving pregnancy rates and treating maternal diseases such as intrauterine growth restriction and preeclampsia. Furthermore, as the implantation process involves numerous signaling pathways common to other systems, this mouse model is a useful biological system for investigating a wide range of biological process beyond reproduction. This includes epithelium-mesenchyme interactions, cell proliferation, differentiation, migration, and invasion in both normal and disease states. Finally, we have pioneered the use of OCT imaging for structural phenotyping of reproductive tract in a novel mutant mouse. Cellular level of resolution, high imaging speed and natural tissue contrast of this approach makes it a unique phenotyping tool. Potentially it can be implemented for in vivo time-lapse analysis and longitudinal studies to investigate functional effects of molecular/genetic manipulations and pharmacological agents, opening a door for variety of innovative studies in reproductive fields.

ACKNOWLEDGMENT

The authors wish to thank Drs. Richard Behringer, Elizabeth Robertson, An Zwijsen, Danny Huylebroeck, and Martin M. Matzuk for the mouse lines for these studies. We are grateful to Drs. Francesco J. Demayo, Jia Peng, Diana Monsivais, and Margeaux Wetendorf for helpful discussions and advice, and Hermann Piard for assistance with mouse genotyping. The α-KRT8 antibody (TROMA I) was developed by P. Brulet and R. Kemler and obtained from the Developmental Studies Hybridoma Bank, which was created by the U.S. National Institutes of Health/National Institute of Child Health and Human Development, Department of Biology, University of Iowa, Iowa City, Iowa.

REFERENCES

1. Zinaman MJ, Clegg ED, Brown CC, O'Connor J, Selevan SG. Estimates of human fertility and pregnancy loss. Fertil Steril 1996; 65:503–509.
2. Norwitz ER, Schust DJ, Fisher SJ. Implantation and the survival of early pregnancy. N Engl J Med 2001; 345:1400–1408.
3. Koot YE, Teklenburg G, Salker MS, Brosens JJ, Macklon NS. Molecular aspects of implantation failure. Biochim Biophys Acta 2012; 1822: 1943–1950.
4. Zhang S, Lin H, Kong S, Wang S, Wang H, Armant DR. Physiological and molecular determinants of embryo implantation. Mol Aspects Med 2013; 34:939–980.
5. Group ECW. Diagnosis and management of the infertile couple: missing information. Hum Reprod Update 2004; 10:295–307.
6. Wang H, Dey SK. Roadmap to embryo implantation: clues from mouse models. Nat Rev Genet 2006; 7:185–199.
7. Cha J, Sun X, Dey SK. Mechanisms of implantation: strategies for successful pregnancy. Nat Med 2012; 18:1754–1767.
8. Massague J. TGFbeta signalling in context. Nat Rev Mol Cell Biol 2012; 13:616–630.
9. Myers M, Pangas SA. Regulatory roles of transforming growth factor beta family members in folliculogenesis. Wiley Interdiscip Rev Syst Biol Med 2010; 2:117–125.
10. Pangas SA. Bone morphogenetic protein signaling transcription factor (SMAD) function in granulosa cells. Mol Cell Endocrinol 2012; 356: 40–47.
11. Li Q. Transforming growth factor beta signaling in uterine development and function. J Anim Sci Biotechnol 2014; 5:52.
12. Jones RL, Stoikos C, Findlay JK, Salamonsen LA. TGF-beta superfamily expression and actions in the endometrium and placenta. Reproduction 2006; 132:217–232.
13. Lee KY, Jeong JW, Wang J, Ma L, Martin JF, Tsai SY, Lydon JP, DeMayo FJ. Bmp2 is critical for the murine uterine decidual response. Mol Cell Biol 2007; 27:5468–5478.
14. Nagashima T, Li Q, Clementi C, Lydon JP, DeMayo FJ, Matzuk MM. BMPR2 is required for postimplantation uterine function and pregnancy maintenance. J Clin Invest 2013; 123:2539–2550.
15. Clementi C, Tripurani SK, Large MJ, Edson MA, Creighton CJ, Hawkins SM, Kovanci E, Kaartinen V, Lydon JP, Pangas SA, DeMayo FJ, Matzuk MM. Activin-like kinase 2 functions in peri-implantation uterine signaling in mice and humans. PLoS Genet 2013; 9:e1003863.
16. Li Q, Agno JE, Edson MA, Nagaraja AK, Nagashima T, Matzuk MM. Transforming growth factor beta receptor type 1 is essential for female reproductive tract integrity and function. PLoS Genet 2011; 7:e1002320.
17. Arnold SJ, Maretto S, Islam A, Bikoff EK, Robertson EJ. Dose-dependent Smad1, Smad5 and Smad8 signaling in the early mouse embryo. Dev Biol 2006; 296:104–118.
18. Pangas SA, Li X, Umans L, Zwijsen A, Huylebroeck D, Gutierrez C, Wang D, Martin JF, Jamin SP, Behringer RR, Robertson EJ, Matzuk MM. Conditional deletion of Smad1 and Smad5 in somatic cells of male and female gonads leads to metastatic tumor development in mice. Mol Cell Biol 2008; 28:248–257.
19. Sirard C, de la Pompa JL, Elia A, Itie A, Mirtsos C, Cheung A, Hahn S, Wakeham A, Schwartz L, Kern SE, Rossant J, Mak TW. The tumor suppressor gene Smad4/Dpc4 is required for gastrulation and later for anterior development of the mouse embryo. Genes Dev 1998; 12:107–119.
20. Tremblay KD, Dunn NR, Robertson EJ. Mouse embryos lacking Smad1 signals display defects in extra-embryonic tissues and germ cell formation. Development 2001; 128:3609–3621.
21. Li X, Tripurani SK, James R, Pangas SA. Minimal fertility defects in mice deficient in oocyte-expressed Smad4. Biol Reprod 2012; 86:1–6.
22. Li Q, Pangas SA, Jorgez CJ, Graff JM, Weinstein M, Matzuk MM. Redundant roles of SMAD2 and SMAD3 in ovarian granulosa cells in vivo. Mol Cell Biol 2008; 28:7001–7011.
23. Middlebrook BS, Eldin K, Li X, Shivasankaran S, Pangas SA. Smad1-Smad5 ovarian conditional knockout mice develop a disease profile similar to the juvenile form of human granulosa cell tumors. Endocrinology 2009; 150:5208–5217.
24. Mansouri-Attia N, Tripurani SK, Gokul N, Piard H, Anderson ML, Eldin K, Pangas SA. TGFbeta signaling promotes juvenile granulosa cell tumorigenesis by suppressing apoptosis. Mol Endocrinol 2014; 28: 1887–1898.
25. Arango NA, Kobayashi A, Wang Y, Jamin SP, Lee HH, Orvis GD, Behringer RR. A mesenchymal perspective of Müllerian duct differentiation and regression in Amhr2-lacZ mice. Mol Reprod Dev 2008; 75: 1154–1162.
26. Jamin SP, Arango NA, Mishina Y, Hanks MC, Behringer RR. Requirement of Bmpr1a for Mullerian duct regression during male sexual development. Nat Genet 2002; 32:408–410.
27. Pangas SA, Li X, Robertson EJ, Matzuk MM. Premature luteinization and cumulus cell defects in ovarian-specific Smad4 knockout mice. Mol Endocrinol 2006; 20:1406–1422.
28. Finn CA, Martin L. Endocrine control of the timing of endometrial sensitivity to a decidual stimulus. Biol Reprod 1972; 7:82–86.
29. Syed SH, Coughlin AJ, Garcia MD, Wang S, West JL, Larin KV, Larina IV. Optical coherence tomography guided microinjections in live mouse embryos: high-resolution targeted manipulation for mouse embryonic research. J Biomed Opt 2015; 20:051020–051020.
30. Livak KJ, Schmittgen TD. Analysis of relative gene expression data using real-time quantitative PCR and the 2(-delta delta C(T)) method. Methods 2001; 25:402–408.

31. Tripurani SK, Cook RW, Eldin KW, Pangas SA. BMP-specific SMADs function as novel repressors of PDGFA and modulate its expression in ovarian granulosa cells and tumors. Oncogene 2013; 32:3877–3885.
32. Mansouri-Attia N, Tripurani SK, Gokul N, Piard H, Anderson ML, Eldin K, Pangas SA. TGFbeta signaling promotes juvenile granulosa cell tumorigenesis by suppressing apoptosis. Mol Endocrinol 2014. me20141217.
33. Nagaraja AK, Andreu-Vieyra C, Franco HL, Ma L, Chen R, Han DY, Zhu H, Agno JE, Gunaratne PH, DeMayo FJ, Matzuk MM. Deletion of Dicer in somatic cells of the female reproductive tract causes sterility. Mol Endocrinol 2008; 22:2336–2352.
34. Daikoku T, Yoshie M, Xie H, Sun X, Cha J, Ellenson LH, Dey SK. Conditional deletion of Tsc1 in the female reproductive tract impedes normal oviductal and uterine function by enhancing mTORC1 signaling in mice. Mol Hum Reprod 2013; 19:463–472.
35. Tanaka Y, Park JH, Tanwar PS, Kaneko-Tarui T, Mittal S, Lee HJ, Teixeira JM. Deletion of tuberous sclerosis 1 in somatic cells of the murine reproductive tract causes female infertility. Endocrinology 2012; 153: 404–416.
36. Miller C, Sassoon DA. Wnt-7a maintains appropriate uterine patterning during the development of the mouse female reproductive tract. Development 1998; 125:3201–3211.
37. Mericskay M, Kitajewski J, Sassoon D. Wnt5a is required for proper epithelial-mesenchymal interactions in the uterus. Development 2004; 131:2061–2072.
38. Mullen RD, Behringer RR. Molecular genetics of Müllerian duct formation, regression and differentiation. Sex Dev 2014; 8:281–296.
39. Raines AM, Adam M, Magella B, Meyer SE, Grimes HL, Dey SK, Potter SS. Recombineering-based dissection of flanking and paralogous Hox gene functions in mouse reproductive tracts. Development 2013; 140: 2942–2952.
40. Stewart CA, Wang Y, Bonilla-Claudio M, Martin JF, Gonzalez G, Taketo MM, Behringer RR. CTNNB1 in mesenchyme regulates epithelial cell differentiation during Müllerian duct and postnatal uterine development. Mol Endocrinol 2013; 27:1442–1454.
41. Migone FF, Ren Y, Cowan RG, Harman RM, Nikitin AY, Quirk SM. Dominant activation of the hedgehog signaling pathway alters development of the female reproductive tract. Genesis 2012; 50:28–40.
42. Wang Z, Wang DZ, Pipes GC, Olson EN. Myocardin is a master regulator of smooth muscle gene expression. Proc Natl Acad Sci U S A 2003; 100: 7129–7134.
43. Long X, Bell RD, Gerthoffer WT, Zlokovic BV, Miano JM. Myocardin is sufficient for a smooth muscle-like contractile phenotype. Arterioscler Thromb Vasc Biol 2008; 28:1505–1510.
44. Lindberg ME, Stodden GR, King ML, MacLean JA II, Mann JL, DeMayo FJ, Lydon JP, Hayashi K. Loss of CDH1 and Pten accelerates cellular invasiveness and angiogenesis in the mouse uterus. Biol Reprod 2013; 89: 8.
45. Franco HL, Dai D, Lee KY, Rubel CA, Roop D, Boerboom D, Jeong JW, Lydon JP, Bagchi IC, Bagchi MK, DeMayo FJ. WNT4 is a key regulator of normal postnatal uterine development and progesterone signaling during embryo implantation and decidualization in the mouse. FASEB J 2011; 25:1176–1187.
46. Gonzalez G, Behringer RR. Dicer is required for female reproductive tract development and fertility in the mouse. Mol Reprod Dev 2009; 76: 678–688.
47. Daikoku T, Jackson L, Besnard V, Whitsett J, Ellenson LH, Dey SK. Cell-specific conditional deletion of Pten in the uterus results in differential phenotypes. Gynecol Oncol 2011; 122:424–429.
48. Monsivais D, Clementi C, Peng J, Titus MM, Barrish JP, Creighton CJ, Lydon JP, DeMayo FJ, Matzuk MM. Uterine ALK3 is essential during the window of implantation. Proc Natl Acad Sci U S A 2015;
49. Peng J, Fullerton PT Jr, Monsivais D, Clementi C, Su GH, Matzuk MM. Uterine activin-like kinase 4 regulates trophoblast development during mouse placentation. Mol Endocrinol 2015; 29:1684–1693.
50. Peng J, Monsivais D, You R, Zhong H, Pangas SA, Matzuk MM. Uterine activin receptor-like kinase 5 is crucial for blastocyst implantation and placental development. Proc Natl Acad Sci U S A 2015; 112:E5098–5107.
51. Wang H, Guo Y, Wang D, Kingsley PJ, Marnett LJ, Das SK, DuBois RN, Dey SK. Aberrant cannabinoid signaling impairs oviductal transport of embryos. Nat Med 2004; 10:1074–1080.
52. Burton JC, Wang S, Larina IV. Dynamic imaging of preimplantation embryos in the murine oviduct. Proc SPIE 2015; 9334:933409.
53. Burton JC, Wang S, Stewart CA, Behringer RR, Larina IV. High-resolution three-dimensional in vivo imaging of mouse oviduct using optical coherence tomography. Biomed Opt Express 2015; 6:2713–2723.
54. Wang S, Burton JC, Behringer RR, Larina IV. In vivo micro-scale tomography of ciliary behavior in the mammalian oviduct. Sci Rep 2015; 5:13216.
55. Stewart CA, Behringer RR. Mouse oviduct development. Results Probl Cell Differ 2012; 55:247–262.
56. Agduhr E. Studies on the structure and development of the bursa ovarica and the tuba uterina in the mouse. Acta Zoologica 1927; 8:1–133.
57. Brody JR, Cunha GR. Histologic, morphometric, and immunocytochemical analysis of myometrial development in rats and mice: I. Normal development. Am J Anat 1989; 186:1–20.
58. Li Q, Kannan A, Das A, Demayo FJ, Hornsby PJ, Young SL, Taylor RN, Bagchi MK, Bagchi IC. WNT4 acts downstream of BMP2 and functions via beta-catenin signaling pathway to regulate human endometrial stromal cell differentiation. Endocrinology 2013; 154:446–457.
59. Li Q, Kannan A, Wang W, Demayo FJ, Taylor RN, Bagchi MK, Bagchi IC. Bone morphogenetic protein 2 functions via a conserved signaling pathway involving Wnt4 to regulate uterine decidualization in the mouse and the human. J Biol Chem 2007; 282:31725–31732.
60. Franco HL, Jeong JW, Tsai SY, Lydon JP, DeMayo FJ. In vivo analysis of progesterone receptor action in the uterus during embryo implantation. Semin Cell Dev Biol 2008; 19:178–186.